UNDRAINED SEISMIC COMPRESSION OF UNSATURATED SAND

By W. Rong, S.M. ASCE[1] and J.S. McCartney, Ph.D., P.E., F. ASCE[2]

ABSTRACT

Unsaturated soils in engineered geostructures like embankments or retaining walls may experience seismic compression during earthquakes due to particle rearrangement associated with large-strain cyclic shearing. Although previous studies have investigated volume changes during drained cyclic shearing of unsaturated soils, undrained cyclic shearing presents a more complex situation. During undrained cyclic shearing, changes in total volume, matric suction, degree of saturation, effective stress, shear modulus, and damping ratio may occur that have complex coupling effects that affect the seismic compression. To better understand these coupling effects, this study presents a series of undrained cyclic simple shear tests on unsaturated sand specimens. The contractile volumetric strains after 200 cycles in these tests were found to vary nonlinearly with degree of saturation. The largest volumetric contraction occurred at a degree of saturation of 0.4 and coincided with the largest decrease in the mean effective stress. The sand specimens followed a wetting-path scanning curve during shearing, with small changes in matric suction. The decrease in mean effective stress during cyclic shearing for all specimens followed the same linear relation with the accumulation of volumetric strains.

INTRODUCTION

Seismic compression of soil layers arises from the accrual of contractive volumetric strains induced by cyclic shearing during an earthquake. Stewart et al. (2001; 2004) found that seismic

[1] Graduate Research Assistant, Department of Structural Engineering, University of California San Diego, La Jolla, CA 92093-0085; Email: w1rong@eng.ucsd.edu
[2] Professor and Department Chair, Department of Structural Engineering, University of California San Diego, La Jolla, CA 92093-0085; Email: mccartney@ucsd.edu

compression was a major cause of to civil infrastructure during the 1994 Northridge, CA earthquake. Unsaturated soils are widely encountered in engineered geostructures like embankments or retaining walls involving compacted backfills, in near-surface natural soil layers above the water table, and even in natural soil deposits below the ground water table where occluded air bubbles are present due to ground water level fluctuations or decomposition of organic materials (Tsukamoto et al. 2002). Furthermore, compacted backfill in highway embankments, bridge abutments, and retaining walls are often designed to remain unsaturated conditions by providing drainage. Although liquefaction of unsaturated soils having high initial degrees of saturation (above 70%) may be an important failure mechanism to consider in seismic analyses (Yoshimi et al. 1989; Unno et al. 2008; Kimoto et al. 2011; Mele et al. 2019), seismic compression may become more relevant for unsaturated soils with lower degrees of saturation (Whang et al. 2000; Stewart et al. 2001; Stewart et al. 2004). Therefore, it is of great importance to understand the seismic compression mechanisms of unsaturated soils as small settlements may affect the normal operation of overlying structures. Contractive volumetric strains of dry and saturated (post-liquefaction) soil layers during earthquake shaking are typically estimated using charts developed by Tokimatsu and Seed (1987) and Ishihara and Yoshimine (1992). These charts include empirical correlations between volumetric strain and cyclic stress ratio for sands having different relative densities and were developed using cyclic simple shear test results for dry and saturated sand from Silver and Seed (1971). However, these charts do not consider seismic compression in the case that liquefaction does not occur during shaking or the impact of the effective stress state in the case the soil is unsaturated.

The drainage condition during cyclic shearing can have a major effect on the evolution and magnitude of seismic compression. Ghayoomi et al. (2011) measured the seismic compression of unsaturated sand layers using centrifuge shaking table experiments and observed partial drainage. Although this may be related to time scaling when using water as the pore fluid in dynamic centrifuge modeling, it emphasizes the importance of considering both drained and undrained conditions when characterizing the seismic compression of unsaturated soils. While several studies have performed drained cyclic simple shear tests on unsaturated sands with the goal of characterizing seismic compression, . Most experience on undrained cyclic shearing behavior of unsaturated soils was gained from cyclic triaxial shearing tests on soils with high initial degrees of saturation which were tested to investigate their liquefaction potential (Okamura and Soga 2006; Unno et al. 2008; Okamura and Noguchi 2009; Kimoto et al. 2011). These studies observed excess pore water and pore air pressure generation during cyclic shearing along with volume change due to compression of air voids and corresponding increases in degree of saturation. These observations are important as coupled changes in pore air and pore water pressures and degree of saturation will lead to changes in the effective stress state (Lu et al. 2010; Rong and McCartney 2020). Further, the shear modulus and damping relationships with cyclic shear strain magnitude are also closely related with the void ratio and effective stress state (Khosravi et al. 2010, Hoyos et al. 2015; Le and Ghayoomi 2017; Dong et al. 2016, 2017), which may play a major role in the evolution in seismic compression.

To better consider the coupling between relevant variables during undrained cyclic shearing of unsaturated sands, this paper presents the results from a series of undrained cyclic simple shear tests performed using an apparatus developed by Rong and McCartney (in review). The evolution in volume, pore air and pore water pressures, and shear stress were monitored during strain-controlled cyclic shearing tests on sand specimens having the same relative density but different initial degrees of saturation in the funicular regime of the SWRC. This information was useful to calculate the degree of saturation, matric suction, effective stress, shear modulus, and damping ratio, which are all needed to understand the mechanisms of seismic compression during undrained cyclic shearing. Specimens were tested in the funicular regime as previous drained cyclic shearing tests by Rong and McCartney (2020) indicate that the seismic compression was greatest in this regime. Specimens in the funicular regime are also expected to have a continuous air phase, which helps experimentally in monitoring the independent evolution in pore air and pore water pressures.

BACKGROUND

Effective Stress in Unsaturated Soils

It is well established that the shear strength, shear modulus, and damping ratio of soils are directly influenced by the effective stress for both saturated and unsaturated soils. Lu et al. (2010) proposed the following form for the effective stress in unsaturated soils:

$$\sigma' = (\sigma - u_a) + \sigma^s \quad (1)$$

where σ is the total normal stress, u_a is the pore air pressure, σ^s is the suction stress. For uncemented soils, Lu et al. (2010) estimated the suction stress by assuming it was equal to the product of the matric suction (equal to the difference between pore air and water pressures, u_a-u_w), and the effective saturation S_e, defined as follows:

$$S_e = \frac{S - S_{res}}{1 - S_{res}} \quad (2)$$

where S is the degree of saturation and S_{res} is the residual saturation. If either the effective saturation or the matric suction is not known, then Lu et al. (2010) noted that they can be related using the van Genuchten (1980) soil water retention curve (SWRC) model:

$$S_e = \left\{\frac{1}{1 + [\alpha_{vG}\,(u_a - u_w)]^{N_{vG}}}\right\}^{1-\frac{1}{N_{vG}}} \quad (3)$$

where a_{vG} and N_{vG} are fitting parameters. If the effective saturation and matric suction are known directly, then their product can be incorporated directly into Equation (1) in place of the suction stress to define the effective stress.

Cyclic Volumetric Behavior of Unsaturated Soils

Experimental studies involving the seismic compression of unsaturated soils have been performed by researchers under drained conditions (Le and Ghayoomi 2017; Rong and McCartney 2020), undrained conditions or partial drainage conditions (Sawada et al. 2006; Unno et al. 2008; Ghayoomi et al. 2011, 2013; Kimoto et al. 2011; Milatz and Grabe 2015), or without consideration of drainage conditions (Hsu and Vucetic 2004; Whang et al. 2004, 2005; Duku et al. 2008; Yee et al. 2014). These studies used a range of experimental techniques ranging from element-scale tests in cyclic simple shear or cyclic triaxial setups to centrifuge scale model testing of soil layers. Of these testing approaches, cyclic simple shear testing permits evaluation of effects of a full reversal of shear strains and careful control of the drainage conditions.

In the drained cyclic simple shear tests of Rong and McCartney (2020), the seismic compression of unsaturated sands in the funicular regime after a large number of cycles was observed to have a log-linear relation with matric suction from the values observed for unsaturated sand. For smaller numbers of cycles (i.e., 200 cycles), they found that specimens with an initial degree of saturation of 0.1 had the lowest seismic compression. Le and Ghayoomi (2017) used a cyclic simple shear device to investigate the effect of degree of saturation and matric suction on the drained seismic compression of Ottawa sand and found that unsaturated sand specimens compressed less than dry or saturated specimens. Specimens with an initial degree of saturation of 0.2 had the lowest seismic compression. Although partial drainage was observed in the centrifuge shaking table tests on unsaturated sand layers reported by Ghayoomi et al. (2011, 2013), the trends in seismic compression with degree of saturation were similar to those reported in these previous studies on drained conditions. However, direct comparisons in trends are difficult as the cyclic shear strain amplitudes in these studies are all different, ranging from values on the order of 0.06% in Le and Ghayoomi (2017) to values on the order of 5% in Rong and McCartney (2020).

Among the studies performed on unsaturated sands in undrained conditions, many were performed on specimens with relatively high initial degrees of saturation and liquefaction was observed (i.e., Okamura and Soga 2006; Unno et al. 2008; Okamura and Noguchi 2009). Sawada et al. (2006) observed volume changes during undrained cyclic triaxial tests on unsaturated sands in the case that they did not liquefy, but did not investigate degrees of saturation below 0.5. Kimoto et al. (2011) performed cyclic triaxial tests on unsaturated sandy soils with three different initial suctions of 0, 10 and 50 kPa in drained and undrained conditions, and observed higher suction led to smaller seismic compression in both drainage conditions. While Unno et al. (2008) and Kimoto et al. (2011) measured the generation of pore water and pore air pressures and changes in volume during cyclic triaxial testing, they did not use them to evaluate the impact of effective stress on seismic compression. As they applied a sequence of increasing cyclic shear strain amplitudes, they did not report the evolution in volumetric strain with cycles for a given amplitude. Other studies like Milatz and Grabe (2015) did not investigate soils under different initial degrees of saturation to understand the impact of this variable on the seismic compression.

Whang et al. (2004) performed cyclic simple shear tests on soils with different fines contents and found that unsaturated conditions only played a major role in the seismic compression of soils with plastic fines. Duku et al. (2008) evaluated the impact of several variables on seismic compression and did not observed a clear effect of degree of saturation on the seismic compression of sands. Yee et al. (2014) evaluated the effect of degree of saturation on the volumetric behavior of compacted sands and found that specimens having intermediate degrees of saturation experienced lower volume change. However, the unsaturated soil specimens in the studies mentioned in this paragraph were formed by tamping and kneading wet soils to reach different initial unsaturated conditions with the same target relative density, which lead to different compaction-induced soil structures that affect their seismic compression behavior.

CYCLIC SIMPLE SHEAR TEST DEVICE FOR UNSATURATED SOILS

The cyclic simple shear device for unsaturated soils developed by Rong and McCartney (in review) was used in this study to perform undrained cyclic simple shear tests on sands under different initial conditions. The specimen housing used to control the initial conditions of soil specimens and to measure the evolution in volume, pore water pressure and pore air pressure during cyclic shearing is shown in Figure 1. The device can accommodate cylindrical specimens having a diameter of 66.7 mm and a height of approximately 20.0 mm, resulting in a height to diameter ratio H/D of approximately 0.3. Although smaller than the maximum H/D ratio given in ASTM D6528, the device was found to provide repeatable results while minimizing the variation in suction across the specimen due to hydrostatic effects. Lateral confinement of the specimen was maintained using a wire-reinforced rubber membrane manufactured by Geonor. This membrane provides lateral constraint and minimizes radial deformation of the specimen during preparation, application of vertical stresses, and cyclic shearing but allows vertical and shear deformation with negligible stiffness from the boundaries. The top platen incorporates a porous stone and recessed grooves for air drainage during suction application or for pore air pressure measurement during undrained shearing. Further, it also incorporates pins that intrude 2 mm into the specimen (10% of the height) to transmit shear stresses from the sliding top cap to the top of the specimen. The pins may affect shear planes near the top of the specimen, but they were found to avoid slippage that was noted in preliminary tests at cyclic shear strains of 10% if these pins were not used. A hydrophobic filter was pushed onto the top platen through the pins, which helps to prevent movement of pore water into the top porous stone while allowing free passage of pore air. Although water could theoretically pass through the holes made by the pins, the use of this hydrophobic filter was found to be effective in preventing water escape from the top of the specimens during undrained shearing for the initial conditions in the funicular regime. The bottom platen incorporates a circular fritted glass disk with an air-entry suction of 50 kPa that transmits water from a hanging column consistent with ASTM D6836 but prevents transmission of air. A hole was drilled in the center of the fritted glass disk to permit a UMS TC5 tensiometer to be passed through the base platen into the lower portion of the soil specimen to monitor changes in pore water pressure during cyclic shearing. The gap between the tensiometer and fritted glass disk was sealed with silicon sealant. The tip of the tensiometer was 3 mm from the base of the specimen (15% of the height), which may affect the formation of shear planes in the specimen but was found to provide a clear understanding of the pore pressure generation in the unsaturated sand specimens. More details can be found in Rong and McCartney (in review).

TEST MATERIAL AND SPECIMEN PREPARATION

The sand used in this study is classified as a well-graded sand (SW) according to the Unified Soil Classification System (USCS) and was previously used in the shaking table experiments on mechanically stabilized earth bridge abutments conducted by Zheng et al. (2018). The particle size distribution curve of the well-graded sand is shown in Figure 2(a), and the mean grain size D_{50} and the effective grain size D_{10} are 0.8 mm and 0.2 mm, respectively. The sand has a coefficient of uniformity of C_u = 6.1 and a coefficient of curvature of C_c = 1.0. The specific gravity is 2.61, and the maximum and minimum void ratios are 0.853 and 0.371, respectively.

The primary wetting and drying paths of the SWRCs for the well-graded sand at a relative density of 0.45 was measured using a hanging column setup that can apply suction higher enough to reach the residual regime of the sand. To measure the SWRCs, a pre-determined mass of dry sand was poured at a constant rate from a funnel into a Büchner funnel having a fritted glass disk with an air-entry suction of 50 kPa at the bottom that was filled with de-aired water. It was found that a target density of 0.45 could be reached reliably without tamping. This specimen preparation approach is similar to that adopted by Tatsuoka et al. (1979). This initially saturated specimen was incrementally desaturated by applying negative water pressures (u_w) to the hanging column while leaving the surface of the specimen open to the atmosphere (air pressure $u_a = 0$). Water outflow was monitored during the primary drainage process, and the tensiometer reading was used to confirm that the target matric suction was reached. Once the outflow of water from the bottom boundary remained constant over a time interval between readings of 30 minutes, the sand specimen was assumed to be at hydraulic equilibrium. During rewetting, water inflow occurred when applied negative water pressure gradually decreased and the degree of saturation was observed to reach a maximum value of 0.52 due to the occlusion of air during rewetting. The equilibrium points on the primary drying path and the primary wetting path are shown in Figure 2(b) along with the fitted van Genuchten (1980) SWRCs. Different regimes of the SWRC defined by Lu and Likos (2004) are also shown in Figure 2(b): the capillary regime where soils remain saturated under negative pore water pressure, the funicular regime where the water phase is continuous, and the residual regime where the water phase is discontinuous. The air-entry suction ψ_{aes} of the sand at the relative density of 0.45 was found to be 1.43 kPa using the graphical approach proposed by Pasha et al. (2015), which considers volume change of the specimen during desaturation. The different initial states of the well-graded sand specimens tested in this study are indicated in Figure 2(b). Tests on near-saturated and dry specimens were also performed for comparison. Although these two extreme conditions cannot be plotted on a logarithmic scale for matric suction but are still shown on the plot as points A and G, respectively. Based on the SWRC fit, the dry specimen ($\theta_w = 0$) is assumed to have a matric suction of 100 kPa. Although the SWRC shown in Figure 2(b) was measured under zero vertical stress which is different from the value of 50 kPa used in the cyclic simple shear testing program, the change in volume during application of the vertical stress in the cyclic simple shear device was relatively small due to the shape of the compression curve at low vertical stresses.

The suction stress characteristic curve (SSCC) for the sand is shown in Figure 2(c) in terms of both degree of saturation and matric suction along with the different initial states of the specimens tested in terms of degree of saturation. The shape of the SSCC indicates that the specimens initially in the funicular region of the SWRC will have a similar suction stress ranging from 1.1 to 1.2 kPa. However, this observation is only true for static conditions as each of the specimens in the funicular range could have different evolutions in matric suction and degree of saturation during undrained cyclic shearing.

Unlike the wet tamping and kneading method used in previous studies involving unsaturated soils (e.g., Whang et al. 2004, 2005; Duku et al. 2008; Yee et al. 2004), which may introduce uncertainty in the soil behavior due to compaction-induced soil structure effects, different unsaturated conditions of sand specimens were achieved by desaturation on the saturated specimens in this study. To prepare the unsaturated sand specimens, saturated specimens were desaturated using the hanging column to reach the target matric suction. Water outflow was monitored during the process, and the tensiometer reading was used to confirm that the target matric suction was reached. Details of the specimen preparation on the simple shear test device can be found in Rong and McCartney (in review) and Rong and McCartney (2020). Once the reading of the tensiometer was constant and the water outflow did not change over 30 minutes, the unsaturated specimen is assumed to be at hydraulic equilibrium and ready for shearing.

EXPERIMENTAL PROCEDURES AND TESTING PROGRAM

Strain-controlled cyclic shearing tests on unsaturated sand specimens with various initial suctions in the funicular regime were performed to evaluate the effect of pore water and pore air on the seismic compression of unsaturated sands in undrained conditions by closing the valve attached to the hanging column on the test device. All the tests were performed under an applied vertical stress of 50 kPa, which represents the stress state of the near-surface unsaturated backfill soils in transportation systems. A cyclic shear strain amplitude of 1% with a was applied for all the tests in the study for N = 200 cycles. This amplitude and number of cycles were found to result in measurable seismic compressions that permit insight into the evolution of significant variables during undrained cyclic shearing. A shear strain rate of 0.833%/min was chosen to ensure the evolution of variables like pore water pressure and pore air pressure can be captured reliably using the instrumentation. Although slower than shear strain rates encountered in earthquakes, the slower rate permits evaluation of the effect of hydro-mechanical variables on the seismic compression. The initial values of specimen height h_0, matric suction ψ_0, degree of saturation S_{r0}, gravimetric water content w_0, volumetric water content θ_{w0} and the gravimetric water content w_f for each specimen after shearing are summarized in Table 1. Many tests were repeated once. During undrained shearing, the valves connecting the bottom of the specimen to the hanging column and the top of the specimen to the atmosphere were closed. During drained shearing, both of these values were open. The inset in Figure 1 shows the values that may change during the drained and undrained tests.

EXPERIMENTAL RESULTS

Typical Test Results during Undrained Cyclic Shearing

Representative undrained cyclic shearing results for an unsaturated sand specimen having an initial suction of 4 kPa are shown in Figure 3. During cyclic shearing, the movement of the top cap was measured to ensure the accurate application of the constant cyclic shear strain amplitude as shown in Figure 3(a). The shear stress required to apply the constant strain in each loading cycle was directly measured using a load cell and was observed to slightly increase with cycles of shearing as shown in Figure 3(b). As the wire-reinforced rubber membrane minimizes radial expansion, the volumetric strain ε_v was assumed to be solely due to changes in height and can be calculated with the known initial specimen height. The volumetric strains shown in Figure 3(c) were found to increase with number of cycles but with a decreased rate. As volume of the specimen contracted with cycles of shearing, the pore water pressure and pore air pressure were observed to increase as shown in Figure 3(d). However, the rate of the change in pore water pressure was higher than the value for pore air pressure, which resulted in a decrease of matric suction with loading cycles as shown in Figure 3(e). This is similar to the findings of Kimoto et al. (2011). Since the water content was constant during undrained shearing, the degree of saturation can be inferred from the volume change, shown in Figure 3(e) as well. The degree of saturation increased gradually with cycles of shearing as volume contracted. The vertical effective stress of the specimen during undrained shearing can be calculated according to Equation (1) using the measured evolutions in pore air pressure, matric suction, and degree of saturation. Since the radial expansion was prevented by the wire-reinforced rubber membrane, the mean effective stress can be obtained by assumed K_0 conditions, shown in Figure 3(f). It was found to decrease gradually with cycles of shearing but and stabilized around N = 140 for this specimen.

Evolutions of Hydro-Mechanical Variables during Undrained Cyclic Shearing

The impacts of initial degree of saturation on the significant hydro-mechanical variables during undrained cyclic shearing are shown in Figure 4. Developments of volumetric strains for representative specimens at the five initial unsaturated conditions are shown in Figure 4(a). The specimen with an initial suction of 3 kPa (C-1) showed the most seismic compression while the specimen with the suction of 10 kPa (F-1) showed the least. The corresponding changes in degree of saturation and matric suction are shown in Figures 4(b) and 4(c), respectively. In all tests, the degree of saturation was observed to increase during undrained cyclic shearing, and the matric suction was observed to decrease. The wettest unsaturated specimen (B-1) showed the most noticeable increase in degree of saturation while the driest unsaturated specimen (F-1) showed the most noticeable decrease in matric suction. Using the evolutions of degree of saturation and matric suction, the evolution in mean effective stresses for all the unsaturated sand specimens was obtained as shown in Figure 4(d). The seismic compression behavior of unsaturated sand specimens during undrained cyclic shearing was found to be closely related with the magnitude of decrease in interparticle stress reflected by the decrease in mean effective stress. Specifically, the unsaturated specimen which showed the smallest volumetric strain (F-1) during undrained cyclic shearing experienced the smallest reduction in mean effective stress, while the unsaturated specimen with the highest volumetric strain (C-1) showed the greatest decrease in the mean effective stress.

Cyclic Responses during Undrained Cyclic Shearing

Representative undrained cyclic shearing responses of an unsaturated sand specimen having an initial suction of 4 kPa are shown in Figure 5. The volumetric strain plotted against cyclic shear strain in Figure 5(a) indicates that the volumetric strain accumulates with cycles of shearing but at a decreasing rate. Evolution of the vertical effective stress is shown in Figure 5(b) with respect to the volumetric strain. The vertical effective stress decreases when the volumetric strain accumulates. This stress path reflects that the specimen is undergoing plastic straining with an evolution in preconsolidation stress, as will be discussed later. The decrease in the vertical effective stress was also plotted against cyclic shear stress in Figure 5(c). Although the vertical effective stress decreased with cycles of shearing, the cyclic shear stress slightly increased. This implies that the loss in interparticle stress may be balanced by the densification associated with cyclic shearing. The slight increase in the cyclic shear stress with cycles can also be identified in the cyclic shear stress-strain hysteretic loops shown in Figure 5(d).

From the shear stress-strain hysteretic loops for the specimens having different initial degrees of saturation, the evolutions in secant shear modulus and damping ratio with number of cycles could be obtained as shown in Figure 6. This figure includes the results for the specimens in near-saturated conditions (A-1) and dry conditions (G-1). As there was no effect of unsaturated conditions on the interparticle stresses between the particles in dry and near-saturated conditions, these two extreme conditions resulted in lower initial secant shear modulus and higher initial damping ratios compared with those for the unsaturated sand specimens, as shown in Figures 6(a) and 6(b), respectively. The secant shear modulus decreased sharply in the first 30 cycles due to the rapid increase in pore water pressures and the resulting decrease in mean effective stress, which agrees well with the findings in the evolution of secant shear modulus for saturated sands at larger cyclic shear strain amplitude by Vucetic and Mortezaie (2015). Despite the decrease in mean effective stress observed in Figure 4(d), the secant shear moduli for the unsaturated sand specimens were observed to increase slightly during cyclic shearing. This increase indicates that the effect of densification due to volume contraction outweighed the effect of the decrease in mean effective stress on the secant shear modulus. Specifically, the unsaturated sand specimens that experienced more seismic compression (C-1, D-1) showed higher secant shear moduli than the unsaturated sand specimens with lower seismic compression (B-1, E-1). Damping ratios were found to decrease rapidly for all the specimens during undrained cyclic shearing over the first 30 cycles but then stabilized. Additionally, the specimens in the near-saturated and dry conditions (A-1, G-1) showed higher damping ratios than the specimens in unsaturated conditions throughout the tests, likely due to the lack of interparticle stresses. The specimens with higher suctions (i.e. specimen F-1) showed lower damping ratios than the ones with lower suctions (i.e., specimen B-1), consistent with the findings of Hoyos et al. (2015) and Le and Ghayoomi (2017) that higher suction leads to lower damping ratio.

Relations between Volume Change and Stress State

The results shown in Figure 5(b) indicate that there may be an approximate linear relation between the volumetric strain and the vertical effective stress for unsaturated sand specimens during undrained cyclic shearing. The volumetric strains plotted against the mean effective stress for specimens with different initial conditions are shown in Figure 7(a). The specimen in near-saturated condition (A-1) experienced negligible volumetric contractions during undrained shearing so the results are not shown. The dry specimen (G-1) had lower initial effective stress as the suction stress was zero, but the effective stress for this specimen decreased during undrained cyclic shearing due to the generation of positive excess pore air pressures. Although the different specimens had different changes in pore air pressure, pore water pressure, and degree of saturation resulting in different amount of matric suction, they all followed a similar linear relationship for several cycles. In some of the tests, the mean effective stress started to stabilize and the relationship became nearly vertical, which was especially the case for the unsaturated specimen with the highest suction of 10 kPa (F-1). The relations between volume change and stress state were replotted in the e-logσ_m' space along with the compression curve from the oedometer test in Figure 7(b). The relationship between mean effective stress and volumetric strain during undrained cyclic shearing moves down and to the left. The only way for this to occur is for plastic strains to accumulate, meaning that the specimens are jumping from one recompression curve to another and the preconsolidation stress is increasing. This hypothetical increase in preconsolidation stress may correspond with the observed increase in shear modulus, as these variables have been shown to be related for unsaturated soils (Khosravi and McCartney 2012).

SYNTHESIZED RESULTS AND DISCUSSION

Dependence of Volume Change on Unsaturated Conditions

To assess the effect of degree of saturation or matric suction on the volume change or seismic compression in undrained conditions, the volumetric strains accumulated after N = 200 cycles were plotted against degree of saturation and matric suction in Figures 8(a) and 8(b), respectively. The solid points in these figures indicate the dependence of the accumulated volumetric strains after N = 200 on the degree of saturation and matric suction after shearing, while the hollow ones indicated the dependence on the initial values prior to shearing. Although the test results for the unsaturated sand specimens with suctions of 3 kPa (corresponding S_{r0} = 0.40) and 10 kPa (corresponding S_{r0} = 0.12) deviated from the trend to some extent, a nonlinear dependence of the volumetric strains on the degree of saturation or matric suction can still be observed with the most seismic compression occurred at the intermediate degrees of saturation or matric suctions evaluated in this study. This is primarily due to the largest decrease in the mean effective stress at the intermediate range of degrees of saturation or suctions during undrained cyclic shearing where the most hydro-mechanical coupling occurred. This observation is contrary to the findings from the cyclic simple shear tests of Whang et al. (2005) and the centrifuge tests of Ghayoomi et al. (2011) that the lowest seismic compression occurs at an intermediate degree of saturation which corresponds to an initial higher modulus. This might be due to the uncontrolled drainage conditions and the different soils tested in these studies. Rong and McCartney (2020) pointed out that drainage conditions for both the pore air and the pore water play an important role in the hydro-mechanical coupling and thus the evolution of the mean effective stress and related seismic compression during cyclic shearing.

Dependence of Changes in Hydro-Mechanical States on the Initial Saturation

In addition to the nonlinear relations shown in Figure 8(a) and 8(b), all the undrained cyclic shearing tests on unsaturated sand specimens led to an increase in degree of saturation and a decrease in matric suction albeit with different magnitudes, as indicated by the solid and hollow points in Figure 8(a) and 8(b), respectively. To evaluate the dependence of these changes in the hydraulic parameters as well as the stress state on the initial degree of saturation, changes in pore pressures, matric suction, degree of saturation and the mean effective stress were analyzed for each of the undrained cyclic shearing tests and the results were summarized and shown in Figure 9. The results in Figure 9(a) indicate that the magnitudes of the changes in pore water and air pressures increased with the degree of saturation. In other words, when subjected to the same cycles of shearing, the wetter the specimen is, the larger changes in both the pore water and pore air pressures can be observed. However, the magnitude of changes in suction decreased with increasing initial degree of saturation during undrained cyclic shearing due to the varying changes in the pore water and pore air pressures for the unsaturated sand specimens with different saturation. Specifically, the pore air pressure generation was found to be more sensitive to the initial degree of saturation than the pore water pressure generation which resulted in the decreased change in suction with the initial degree of saturation. The dependence of the change in degree of saturation during cyclic shearing in terms of the initial saturation is shown in Figure 9(b). It is obvious in this figure that the change in degree of saturation was highly related with the initial saturation, with larger positive changes in degree of saturation for initially wetter specimens. With the known changes in matric suction and degree of saturation, the decreases in the mean effective stress for different initial degrees of saturation are shown in Figure 9(c). Wetter specimens with higher initial degrees of saturation experienced larger decreases in mean effective stress during undrained cyclic shearing.

Dependence of Changes in Hydro-Mechanical States on the Volume Change

Changes in pore pressures, matric suction, degree of saturation and the mean effective stress were also analyzed for each of the cyclic shearing tests as a function of the accumulated volumetric strains after 200 cycles of undrained cyclic shearing, and the results were summarized and shown in Figure 10. The results in Figure 10(a) indicate that larger volumetric contractions resulted in higher increases in both pore water pressure and pore air pressure. However, due to the different rates of increase in the pore air and pore water pressures a decrease in the change of matric suction was observed. Accordingly, more seismic compression will not necessarily lead to a larger decrease in suction. Additionally, the change of suction during undrained cyclic shearing not only depends on the volumetric contraction or seismic compression, but also highly related with the initial unsaturated condition. Greater volumetric contractions resulted in larger increases in degree of saturation as shown in Figure 10(b), which is expected as these variables are directly related during undrained shearing. Regardless of the initial unsaturated condition in the specimen, more volumetric contraction or seismic compression during undrained cyclic shearing led to a larger decrease in the mean effective stress, as shown in Figure 10(c), which means that volumetric contraction was closely related to the decrease in interparticle stress for unsaturated sand specimens during undrained cyclic shearing.

Comparison with Drained Cyclic Shearing Tests and Discussions

The degree of saturation and matric suction of the unsaturated sand specimens at the end of undrained cyclic shearing (after N = 200) are plotted in Figure 11(a), along with the SWRC and the initial conditions before shearing. The hydraulic states at the end of drained cyclic shearing after N = 200 from Rong and McCartney (2020) are also shown for comparison. Unlike the drained cyclic shearing tests, which led to an upward movement of the SWRC (the same suction value but with an increased degree of saturation), the undrained cyclic shearing caused the unsaturated sand specimens to follow a wetting path along a scanning curve. This occurred due to an increase in degree of saturation and a decrease in matric suction during cyclic shearing. The accumulated volumetric strains after N = 200 were shown against the mean effective stress at the end of both the drained and the undrained cyclic shearing tests in Figure 11(b) to quantify the relation between the volumetric strain and the stress state. For drained cyclic shearing, the mean effective stress for unsaturated sand specimens with different initial suctions along the test did not vary significantly, and the volumetric strains primarily depended on the initial stress state. However, for undrained cyclic shearing there was a stronger relation between the volumetric strain and the evolution in the stress state, as larger seismic compressions were observed for specimens with lower mean effective stress at the end of shearing. This means that the initial state (i.e. the volume of pore air that is susceptible to compression) as well as the evolution of the stress state play critical roles in seismic compression during undrained shearing.

The accumulated volumetric strains in the unsaturated sand specimens with different initial degrees of saturation in the funicular regime during undrained cyclic shearing are shown in Figure

12 as a function of the degree of saturation (at the beginning of shearing and after N=200), along with the drained cyclic shearing experimental results from Rong and McCartney (2020). Although the drained seismic compression model proposed in Rong and McCartney (2020) is suitable for predicting the ultimate or stabilized seismic compression of unsaturated soils subjected to large-strain cyclic shearing which acts as the worst scenario for design, predictions using the model by assuming N = 200 are also shown in Figure 12 for comparison. Shifts in the degree of saturation are not significant for the well-graded unsaturated sand specimens initially in the funicular regime of the SWRC during drained and undrained cyclic shearing tests over the number of cycles evaluated (N = 200). Although the drained seismic compression results followed an approximately linear decreasing relation with increasing degree of saturation, the undrained seismic compression results showed a nonlinear dependence on the degree of saturation. The greatest seismic compression occurring at the intermediate degrees of saturation (0.30 to 0.45) where the most hydro-mechanical coupling occurs during undrained cyclic shearing. In other words, specimens in this intermediate degree of saturation range have a sufficient amount of air that can collapse during cyclic shearing, but also a sufficient amount of water that can pressurize and lead to a decrease in effective stress.

CONCLUSIONS

Strain-controlled cyclic simple shear tests were performed in this study to investigate the effect of unsaturated conditions on the seismic compression of sands in undrained conditions (no inflow or outflow of air or water). Unlike the results in drained conditions (constant suction with free flow of air and water), seismic compression of unsaturated sand specimens initially in the funicular regime showed a nonlinear relation with degree of saturation. The evolution in mean effective stress resulting from hydro-mechanical coupling played a significant role on the magnitude of seismic compression encountered during undrained cyclic shearing. The main conclusions are summarized as follows:

- For sand specimens initially in the funicular regime, undrained cyclic shearing resulted in volumetric contraction, an increase in degree of saturation, and pressurization of both the pore water and pore air. The differential rates of pressurization of the pore air and pore water led to a decrease in matric suction, which when combined with the increase in degree of saturation led to a decrease in mean effective stress during undrained cyclic shearing for all the specimens tested. Larger volumetric strains occurred in specimens that experienced larger increases in pore water pressure, pore air pressure, and degree of saturation during undrained cyclic shearing.
- The seismic compression of unsaturated sands during undrained cyclic shearing is highly related to the evolution of the mean effective stress. For the well-graded sand investigated in this study, specimens with higher initial degrees of saturation experienced higher increases in pore water pressure, pore air pressure, degree of saturation and the resulting mean effective stress in undrained cyclic shearing. The change in pore air pressure was found to be more sensitive to the initial saturation than the change in pore water pressure, resulting in a decrease in matric suction for specimens with greater initial degrees of saturation.
- Although the changes in degree of saturation and matric suction are not significant during undrained cyclic shearing, the well-graded sand specimens were observed to follow a wetting path scanning curve away from the initial points on the drying path SWRC, which greatly influenced the stress state and thus the seismic compression.
- Different from the trends in seismic compression observed during drained cyclic shearing, the seismic compression observed during undrained cyclic shearing showed a nonlinear

dependence on the degree of saturation with the greatest seismic compression occurring at the intermediate degrees of saturation (0.30 to 0.45).

DATA AVAILABILITY STATEMENT

All data, models, and code generated or used during the study appear in the submitted article.

ACKNOWLEDGMENTS

The authors would like to acknowledge partial financial support provided by the Department of Transportation in California (Caltrans) Project 65A0556 and from the University of California San Diego Academic Senate Grant A050757.

REFERENCES

ASTM D6528 (2017). Standard Test Method for Consolidated Undrained Direct Simple Shear Testing of Cohesive Soils. ASTM International. West Conshohocken, PA.

ASTM D6836 (2016). Standard Test Methods for Determination of the Soil Water Characteristic Curve for Desorption Using Hanging Column, Pressure Extractor, Chilled Mirror Hygrometer, or Centrifuge. ASTM International. West Conshohocken, PA.

Duku, P.M., Stewart, J.P., Whang, D.H., and Yee, E. (2008). "Volumetric strains of clean sands subject to cyclic loads." J. of Geotech. and Geoenv. Eng., 134(8), 1073-1085.

Dong, Y., Lu, N., and McCartney, J.S. (2016). "Unified model for small-strain shear modulus of variably saturated soil." J. of Geotech. and Geoenv. Eng., 142(9), 04016039.

Ghayoomi, M., McCartney, J.S., and Ko, H.Y. (2011). "Centrifuge test to assess the seismic compression of partially saturated sand layers." Geotechnical Testing Journal, 34(4), 321-331.

Ghayoomi, M., McCartney, J.S., and Ko, H.Y. (2013). "Empirical methodology to estimate seismically induced settlement of partially saturated sand." J. of Geotech. and Geoenv. Eng., 139(3), 367-376.

Hsu, C.C. and Vucetic, M. (2004). “Volumetric threshold shear strain for cyclic settlement.” J. of Geotech. and Geoenv. Eng., 130(1), 58-70.

Hoyos, L.R., Suescún-Florez, E.A., and Puppala, A.J. (2015). “Stiffness of intermediate unsaturated soil from simultaneous suction-controlled resonant column and bender element testing.” Engineering Geology, 188, 10-28.

Ishihara, K. and Yoshimine, M. (1992). “Evaluation of settlements in sand deposits following liquefaction during earthquakes.” Soils and Foundations, 32(1), 173-188.

Khosravi, A., Ghayoomi, M., McCartney, J.S., and Ko, H.Y. (2010). “Impact of effective stress on the dynamic shear modulus of unsaturated sand.” GeoFlorida 2010, 410-419.

Khosravi, A. and McCartney, J.S. (2012). “Impact of hydraulic hysteresis on the small-strain shear modulus of unsaturated soils.” ASCE Journal of Geotechnical and Geoenvironmental Engineering. 138(11), 1326–1333.

Kimoto, S., Oka, F., Fukutani, J., Yabuki, T., and Nakashima, K. (2011). “Monotonic and cyclic behavior of unsaturated sandy soil under drained and fully undrained conditions.” Soils and Foundations, 51(4), 663-681.

Lu, N. and Likos, W.J. (2004). Unsaturated Soil Mechanics. Wiley and Sons. New York.

Lu, N., Godt, J.W., and Wu, D.T. (2010). “A closed form equation for effective stress in unsaturated soil.” Water Resources Research, 46(5), 55-65.

Le, K. N. and Ghayoomi, M. (2017). “Cyclic direct simple shear test to measure strain-dependent dynamic properties of unsaturated sand.” Geotechnical Testing Journal, 40(3), 381-395.

Milatz, M. and Grabe, J. (2015). “A new simple shear apparatus and testing method for unsaturated sands.” Geotechnical Testing Journal, 38(1), 9-22.

Okamura, M. and Soga, Y. (2006). "Effects of pore fluid compressibility on liquefaction resistance of partially saturated sand." Soils and Foundations, 46(5), 695-700.

Okamura, M. and Noguchi, K. (2009). "Liquefaction resistances of unsaturated non-plastic silt." Soils and Foundations, 49(2), 221-229.

Pasha, A.Y., Khoshghalb, A., and Khalili, N. (2015). "Pitfalls in interpretation of gravimetric water content–based soil-water characteristic curve for deformable porous media." International Journal of Geomechanics, 16(6), D4015004.

Rong, W. and McCartney, J.S. (2020). "Drained seismic compression of unsaturated sand." ASCE Journal of Geotechnical and Geoenvironmental Engineering. 10.1061/(ASCE)GT.1943-5606.0002251.

Rong, W. and McCartney, J.S. (in review) "Methodology to characterize the seismic compression of unsaturated sands under different drainage conditions." ASTM Geotechnical Testing Journal. In 2nd review.

Silver, M.L., and Seed, H.B. (1971). "Deformation characteristics of sands under cyclic loading." Journal of Soil Mechanics and Foundations Division, 97(8), 1081-1098.

Stewart, J.P., Bray, J.D., McMahon, D.J., Smith, P.M., and Kropp, A.L. (2001). "Seismic performance of hillside fills." J. of Geotech. and Geoenv. Eng., 127(11), 905-919.

Stewart, J.P., Smith, P.M., Whang, D.H., and Bray, J.D. (2004). "Seismic compression of two compacted earth fills shaken by the 1994 Northridge earthquake." J. of Geotech. and Geoenv. Eng., 130(5), 461-476.

Sawada, S., Tsukamoto, Y., and Ishihara, K. (2006). "Residual deformation characteristics of partially saturated sandy soils subjected to seismic excitation." Soil Dynamics and Earthquake Engineering, 26(2-4), 175-182.

Tatsuoka, F., Iwasaki, T., Yoshida, S., Fukushima, S., and Sudo, H. (1979). “Shear modulus and damping by drained tests on clean sand specimens reconstituted by various methods.” Soils and Foundations, 19(1), 39-54.

Tokimatsu, K., and Seed, H.B. (1987). “Evaluation of settlements in sands due to earthquake shaking.” Journal of Geotechnical Engineering, 113(8), 861-878.

Tsukamoto, Y., Ishihara, K., Nakazawa, H., Kamada, K., and Huang, Y. (2002). “Resistance of partly saturated sand to liquefaction with reference to longitudinal and shear wave velocities.” Soils and Foundations, 42(6), 93-104.

Unno, T., Kazama, M., Uzuoka, R., and Sento, N. (2008). “Liquefaction of unsaturated sand considering the pore air pressure and volume compressibility of the soil particle skeleton.” Soils and Foundations, 48(1), 87-99.

van Genuchten, M.T. (1980). “A closed-form equation for predicting the hydraulic conductivity of unsaturated soils.” Soil Science Society of America Journal, 44(5), 892-898.

Vucetic, M., and Mortezaie, A. (2015). “Cyclic secant shear modulus versus pore water pressure in sands at small cyclic strains.” Soil Dynamics and Earthquake Engineering, 70, 60-72.

Whang, D.H., Stewart, J.P., and Bray, J.D. (2004). “Effect of compaction conditions on the seismic compression of compacted fill soils.” Geotechnical Testing Journal, 27(4), 1-9.

Whang, D.H., Moyneur, M.S., Duku, P., and Stewart, J.P. (2005). “Seismic compression behavior of nonplastic silty sands.” Proc., Int. Symp. on Advanced Experimental Unsaturated Soil Mechanics, A. Tarantino, E. Romero, and Y.J. Cui, eds., Balkema, Lisse, Netherlands, 257–263.

Yee, E., Duku, P.M., and Stewart, J.P. (2014). “Cyclic volumetric strain behavior of sands with fines of low plasticity.” Journal of Geotechnical and Geoenvironmental Engineering, 140(4), 04013042.

Zheng, Y., Sander, A.C., Rong, W., Fox, P.J., Shing, P., and McCartney, J.S. (2018). “Shaking table test of a half-scale geosynthetic-reinforced soil bridge abutment.” Geotechnical Testing Journal, 41(1), 171-192.

TABLE 1: Test program for the well-graded sand at an initial relative density of 0.45

Specimen No.	Initial specimen height, h_0 (mm)	Initial matric suction, ψ_0 (kPa)	Initial degree of saturation, S_{r0} (m^3/m^3)	Initial gravimetric water content, w_0 (kg/kg)	Initial volumetric water content, θ_{w0} (m^3/m^3)	Final gravimetric water content, w_f (kg/kg)
A-1	20.04	0.04	0.940	0.236	0.379	0.238
B-1	20.03	2.05	0.558	0.135	0.214	0.136
B-2	19.85	2.09	0.549	0.133	0.211	0.133
C-1	19.95	3.01	0.400	0.098	0.156	0.097
C-2	19.39	2.99	0.401	0.098	0.157	0.097
D-1	19.96	3.99	0.308	0.075	0.119	0.075
D-2	19.76	3.96	0.310	0.075	0.120	0.074
E-1	19.89	5.98	0.204	0.049	0.079	0.047
E-2	19.78	6.03	0.200	0.049	0.078	0.049
F-1	19.92	9.98	0.117	0.029	0.046	0.027
F-2	19.78	10.02	0.117	0.029	0.046	0.030
G-1	19.94	100.00*	0.000	0.000	0.000	0.000

*The dry specimen was assumed to have a suction value of 100 kPa corresponding to residual conditions

Fig 1

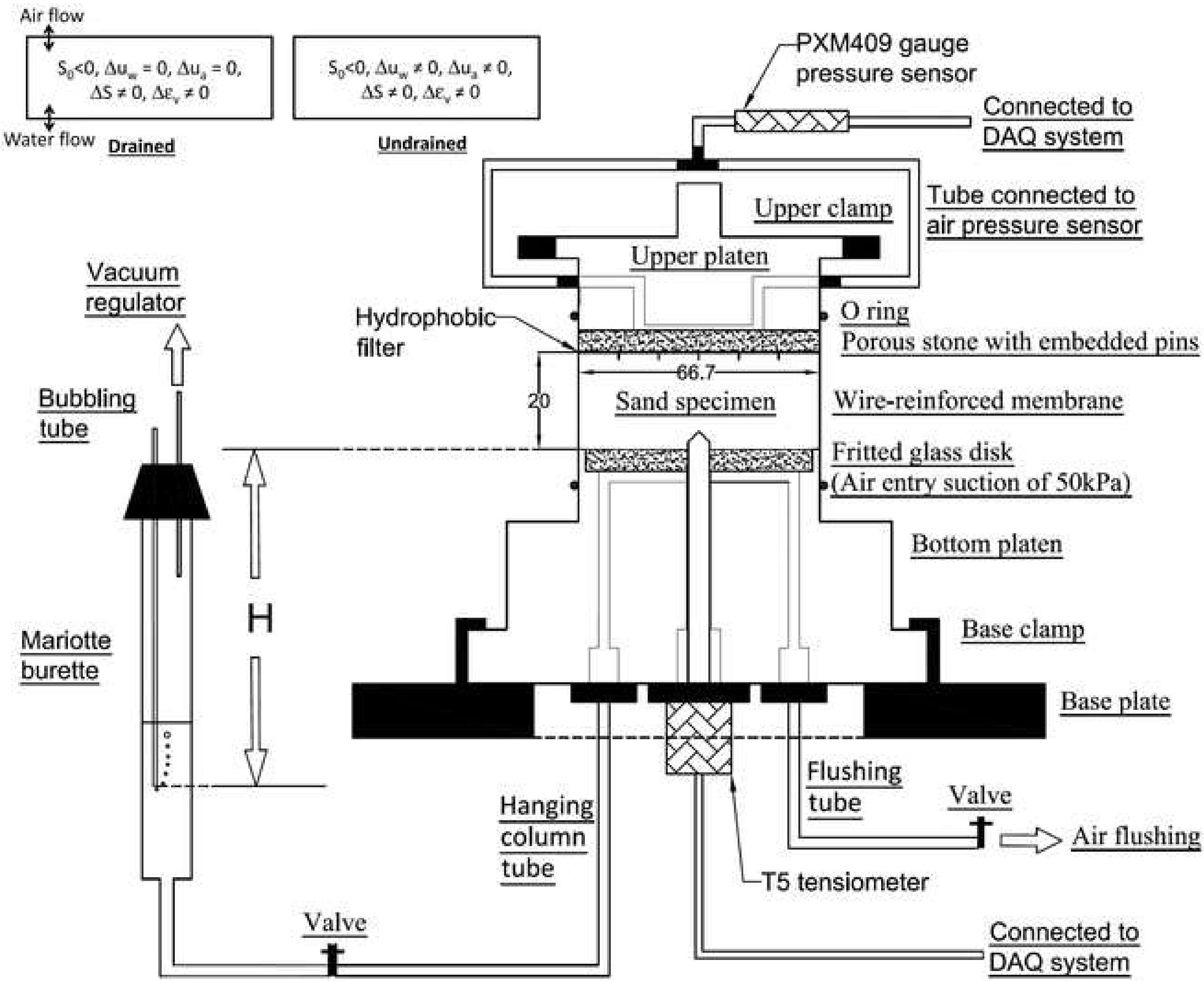

Air flow
$S_0<0, \Delta u_w = 0, \Delta u_a = 0, \Delta S \neq 0, \Delta \varepsilon_v \neq 0$
Water flow
Drained
$S_0<0, \Delta u_w \neq 0, \Delta u_a \neq 0, \Delta S \neq 0, \Delta \varepsilon_v \neq 0$
Undrained
PXM409 gauge pressure sensor
Connected to DAQ system
Upper clamp
Tube connected to air pressure sensor
Upper platen
Vacuum regulator
Hydrophobic filter
O ring
Porous stone with embedded pins
66.7
20
Sand specimen
Bubbling tube
Wire-reinforced membrane
Fritted glass disk
(Air entry suction of 50kPa)
Bottom platen
H
Mariotte burette
Base clamp
Base plate
Flushing tube
Valve
Air flushing
Hanging column tube
T5 tensiometer
Valve
Connected to DAQ system

Fig 2 Click here to access/download;Figure;FIG 2.tif

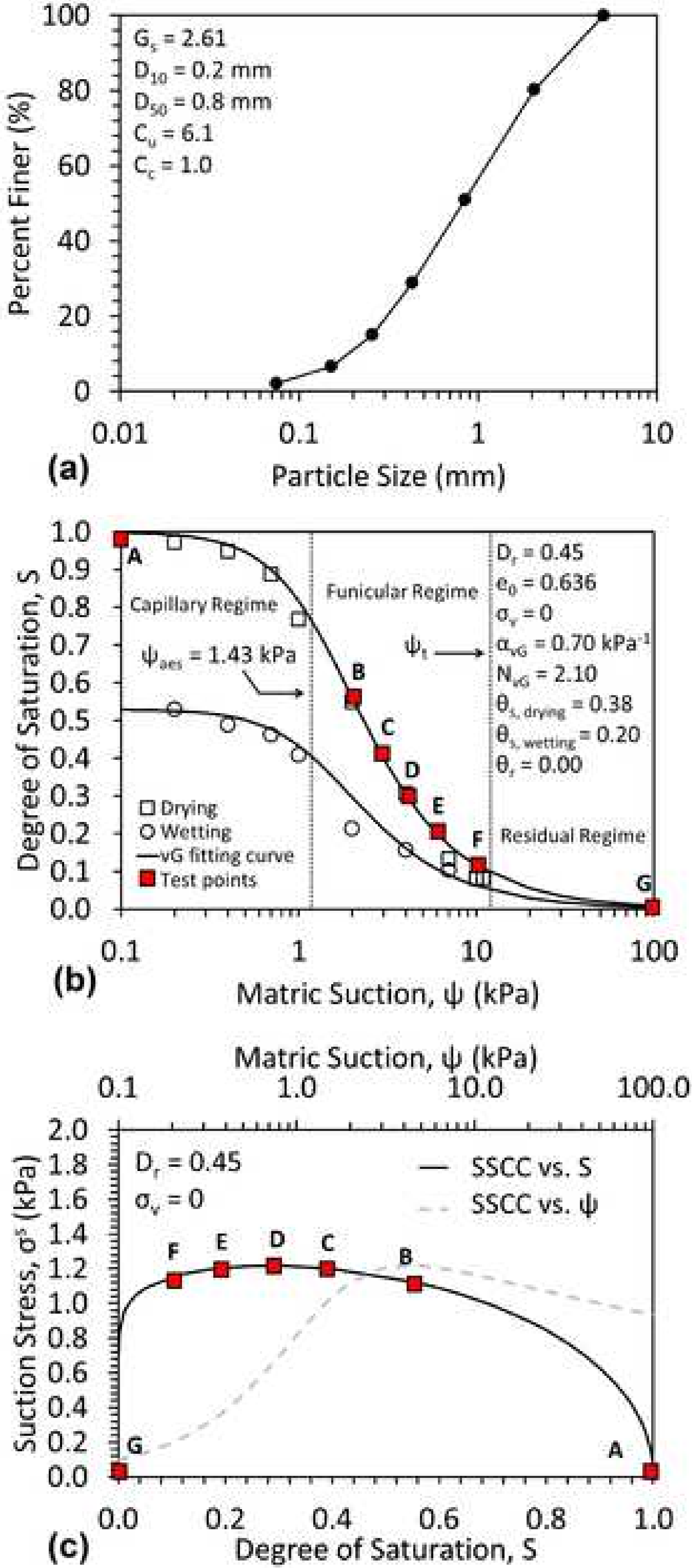

Fig 3

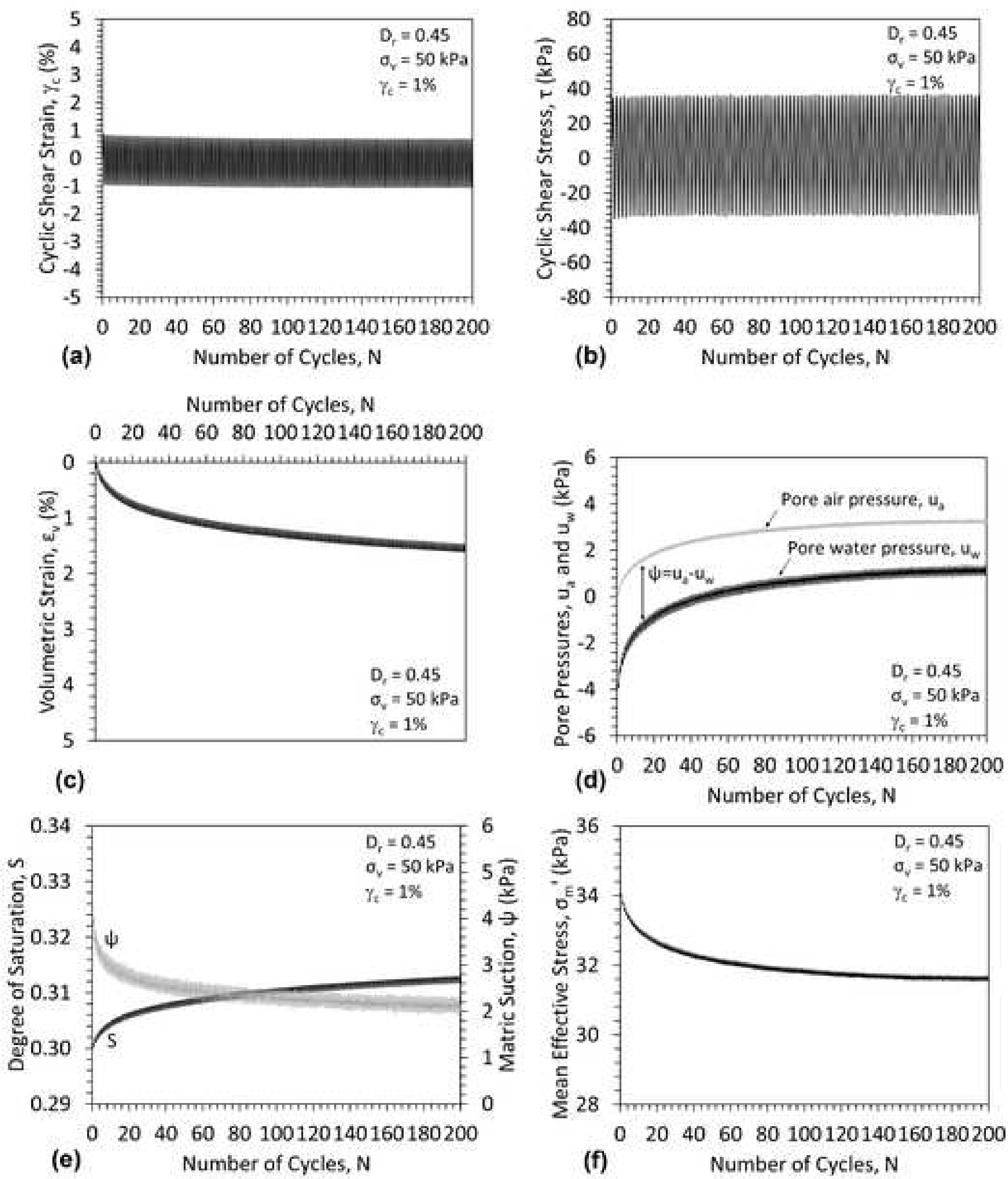

Cyclic Shear Strain, γ_c (%)
D_r = 0.45
σ_v = 50 kPa
γ_c = 1%
Number of Cycles, N
(a)
Cyclic Shear Stress, τ (kPa)
(b)
Volumetric Strain, ε_v (%)
(c)
Pore Pressures, u_a and u_w (kPa)
Pore air pressure, u_a
Pore water pressure, u_w
$\psi = u_a - u_w$
(d)
Degree of Saturation, S
Matric Suction, ψ (kPa)
(e)
Mean Effective Stress, σ_m' (kPa)
(f)

Fig 4

Click here to access/download;Figure;FIG 4.tif

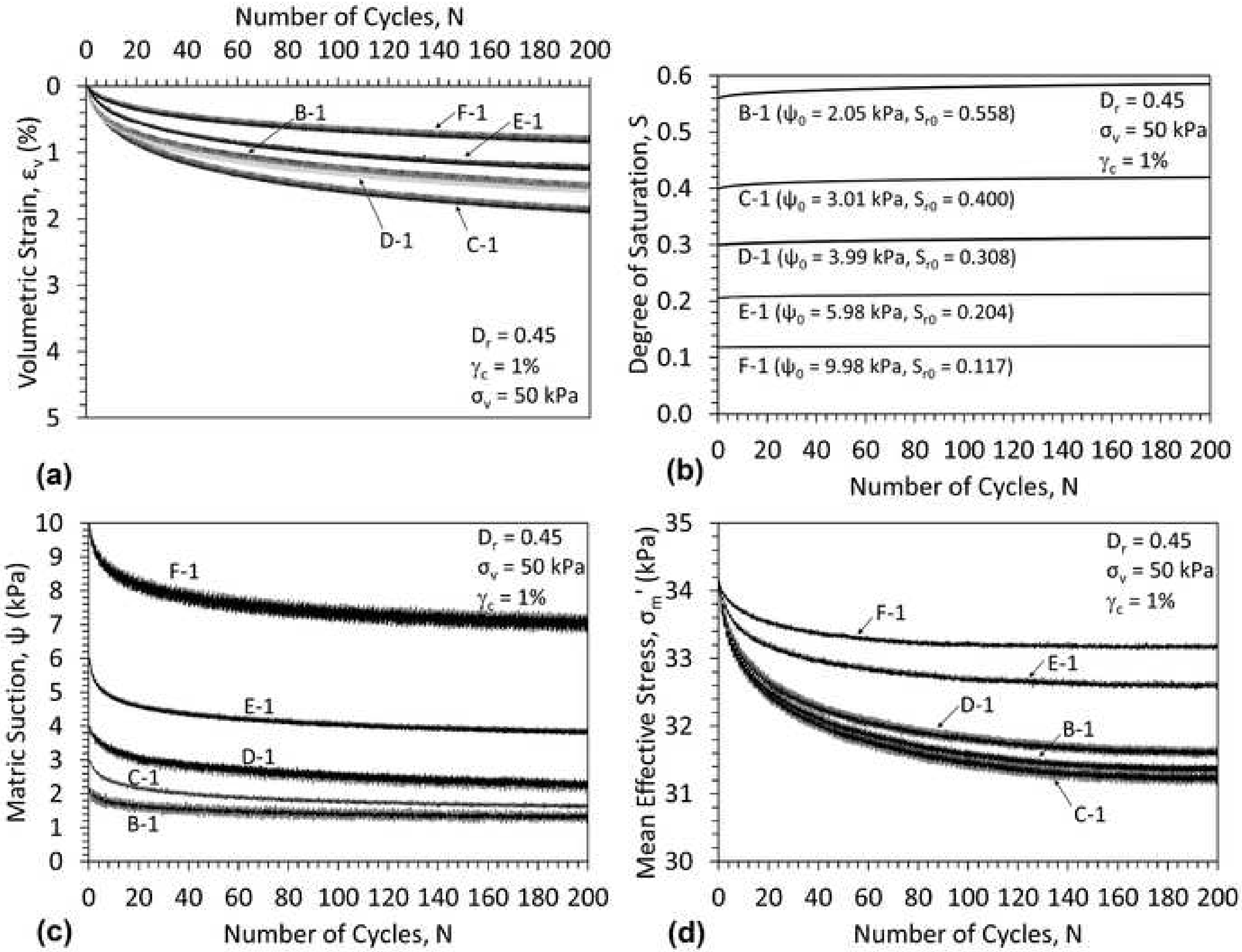

Fig 5

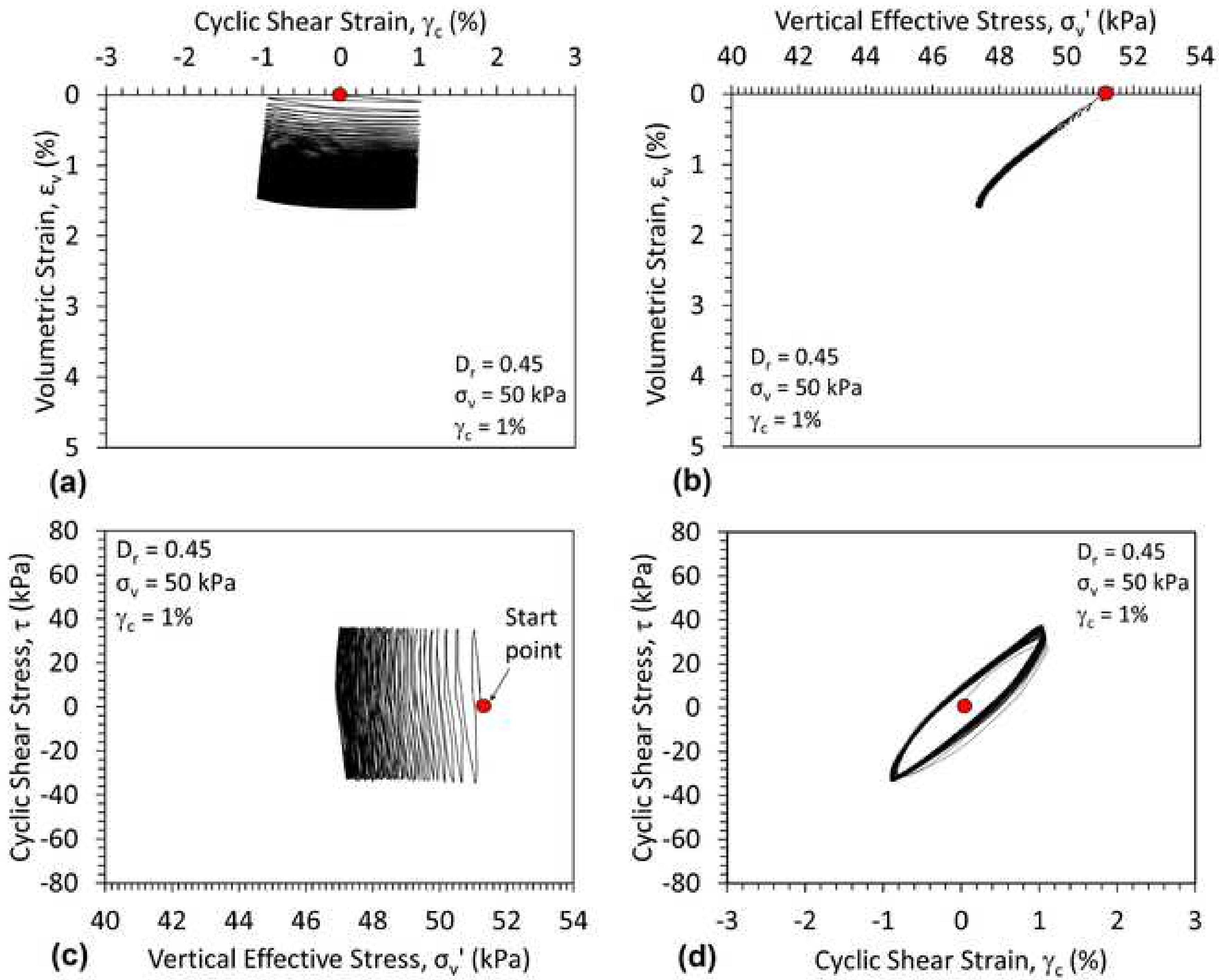
Cyclic Shear Strain, γc (%)
-3 -2 -1 0 1 2 3
0 1 2 3 4 5
Volumetric Strain, εv (%)
Dr = 0.45
σv = 50 kPa
γc = 1%
(a)
Vertical Effective Stress, σv' (kPa)
40 42 44 46 48 50 52 54
0 1 2 3 4 5
Volumetric Strain, εv (%)
Dr = 0.45
σv = 50 kPa
γc = 1%
(b)
80 60 40 20 0 -20 -40 -60 -80
Cyclic Shear Stress, τ (kPa)
Dr = 0.45
σv = 50 kPa
γc = 1%
Start point
40 42 44 46 48 50 52 54
(c)
Vertical Effective Stress, σv' (kPa)
80 60 40 20 0 -20 -40 -60 -80
Cyclic Shear Stress, τ (kPa)
Dr = 0.45
σv = 50 kPa
γc = 1%
-3 -2 -1 0 1 2 3
(d)
Cyclic Shear Strain, γc (%)

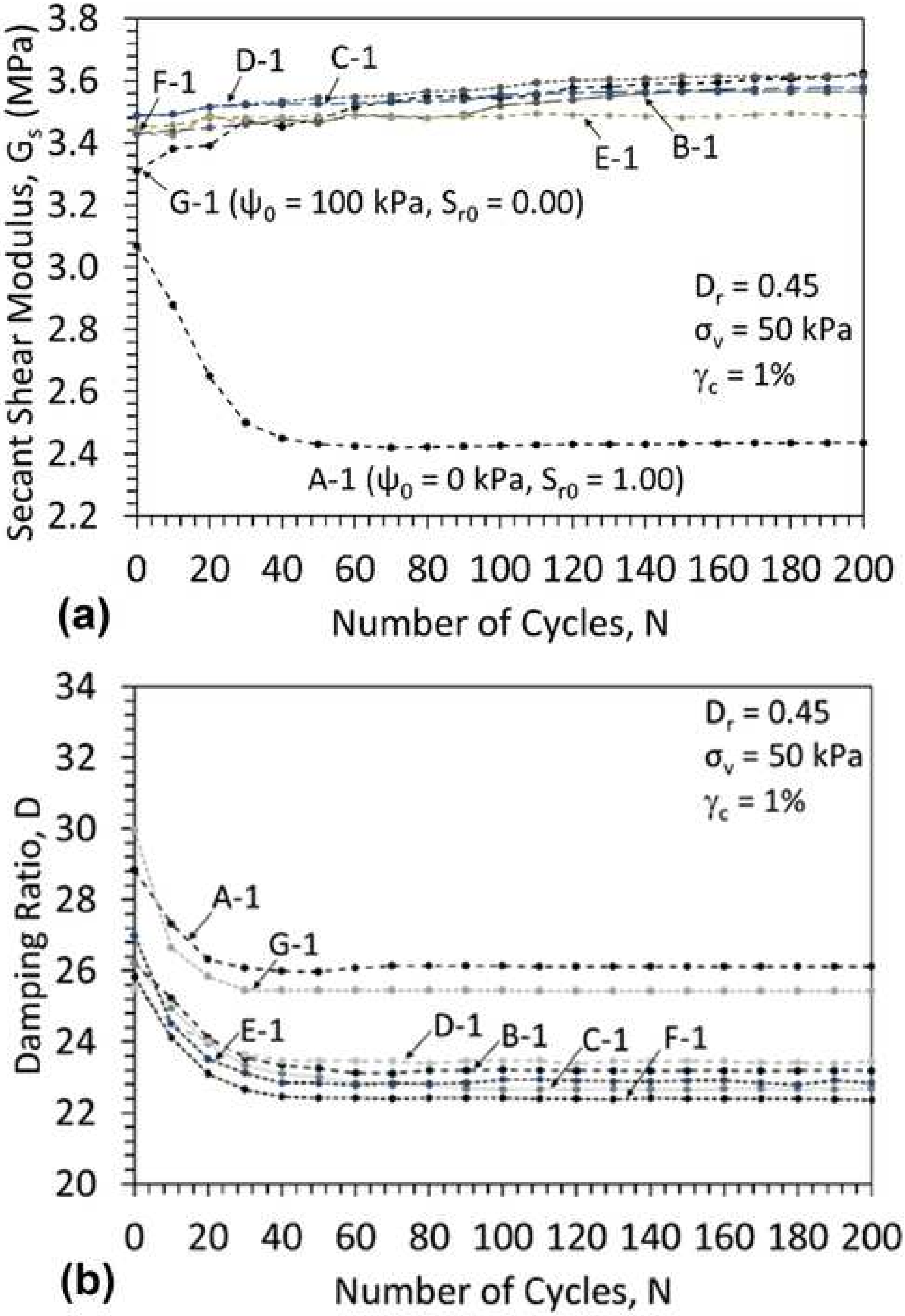
Secant Shear Modulus, G_s (MPa)
3.8
3.6
3.4
3.2
3.0
2.8
2.6
2.4
2.2
F-1
D-1
C-1
E-1
B-1
G-1 (ψ_0 = 100 kPa, S_{r0} = 0.00)
D_r = 0.45
σ_v = 50 kPa
γ_c = 1%
A-1 (ψ_0 = 0 kPa, S_{r0} = 1.00)
0 20 40 60 80 100 120 140 160 180 200
(a)
Number of Cycles, N
Damping Ratio, D
34
32
30
28
26
24
22
20
D_r = 0.45
σ_v = 50 kPa
γ_c = 1%
A-1
G-1
E-1
D-1
B-1
C-1
F-1
0 20 40 60 80 100 120 140 160 180 200
(b)
Number of Cycles, N

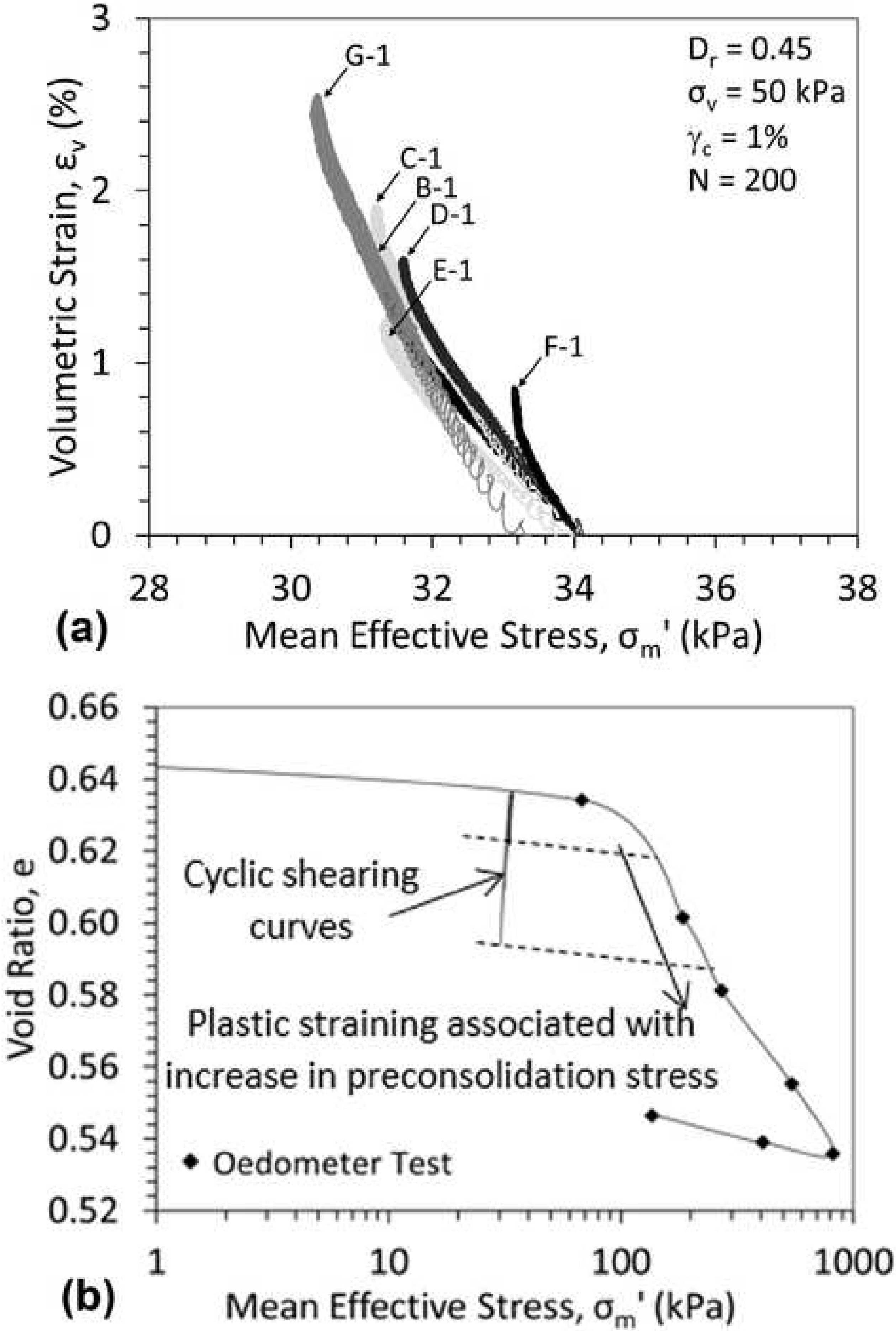

Volumetric Strain, εv (%)
3
2
1
0
28
30
32
34
36
38
Mean Effective Stress, σm' (kPa)
(a)
G-1
C-1
B-1
D-1
E-1
F-1
Dr = 0.45
σv = 50 kPa
γc = 1%
N = 200
Void Ratio, e
0.66
0.64
0.62
0.60
0.58
0.56
0.54
0.52
1
10
100
1000
Mean Effective Stress, σm' (kPa)
(b)
Cyclic shearing curves
Plastic straining associated with increase in preconsolidation stress
Oedometer Test

Fig 8 Click here to access/download;Figure;FIG 8.tif

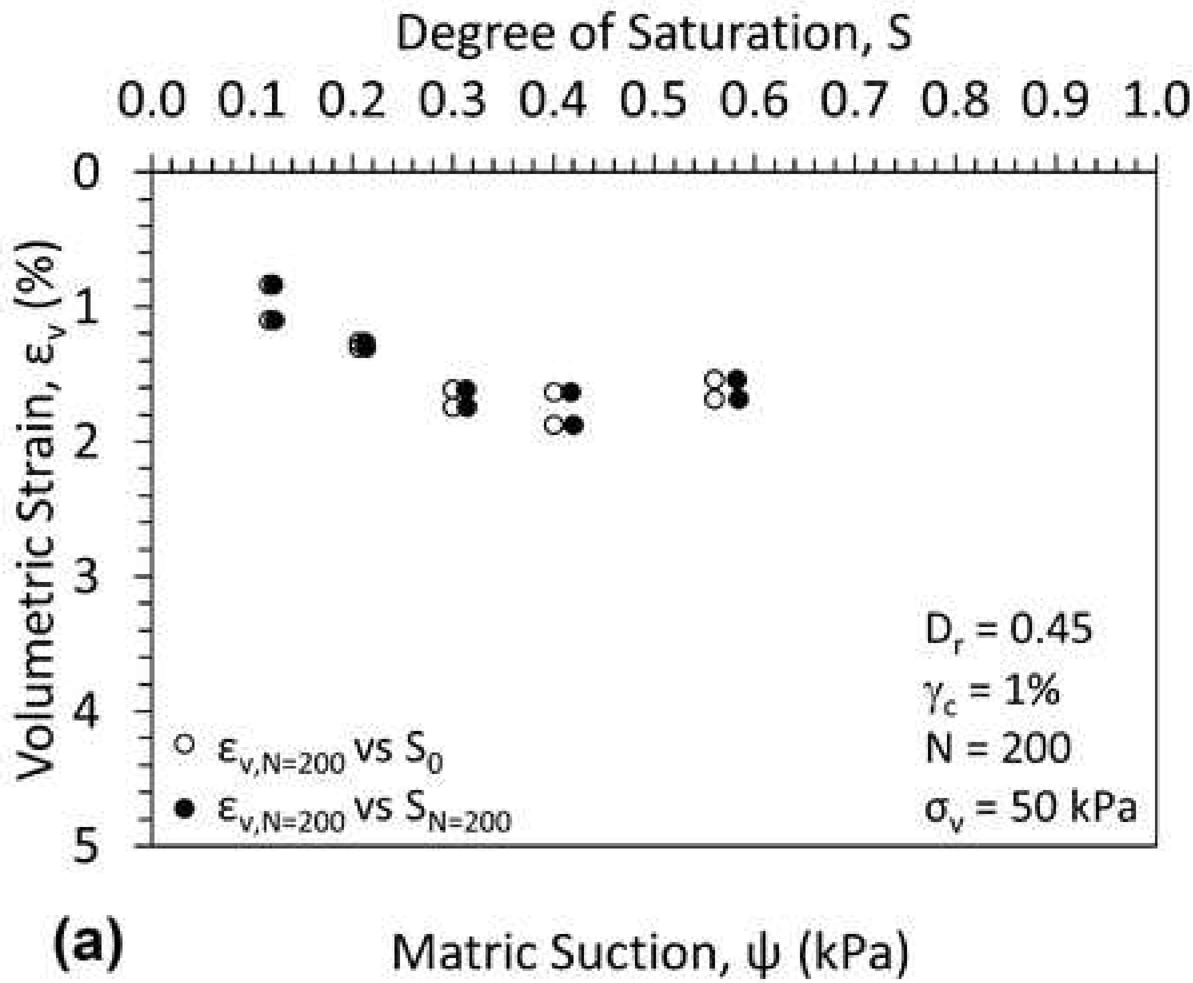

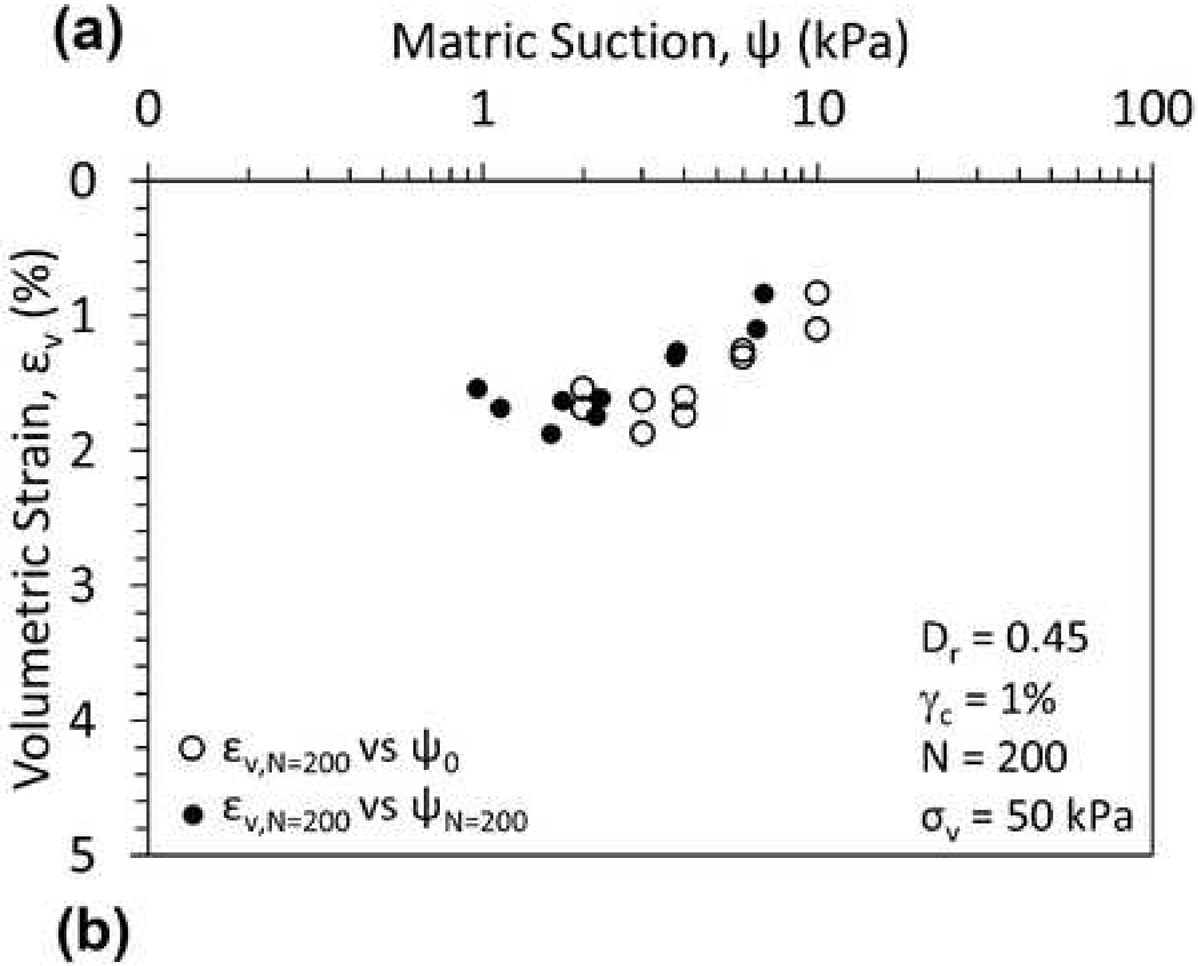

Fig 9

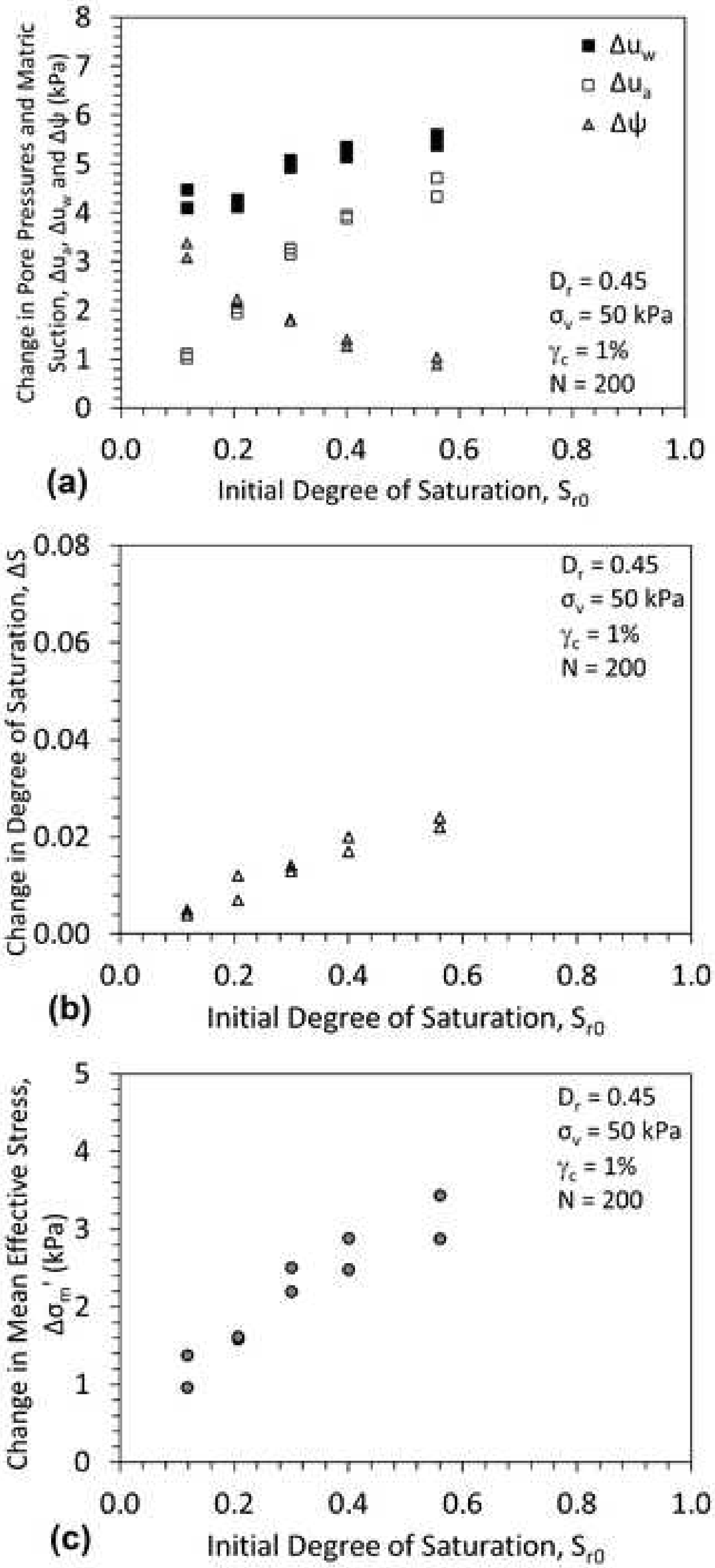

Change in Pore Pressures and Matric Suction, Δu_a, Δu_w, and Δψ (kPa)
Δu_w
Δu_a
Δψ
D_r = 0.45
σ_v = 50 kPa
γ_c = 1%
N = 200
(a)
Initial Degree of Saturation, S_r0
Change in Degree of Saturation, ΔS
D_r = 0.45
σ_v = 50 kPa
γ_c = 1%
N = 200
(b)
Initial Degree of Saturation, S_r0
Change in Mean Effective Stress, Δσ_m' (kPa)
D_r = 0.45
σ_v = 50 kPa
γ_c = 1%
N = 200
(c)
Initial Degree of Saturation, S_r0

Fig 10

Click here to access/download;Figure;FIG 10.tif

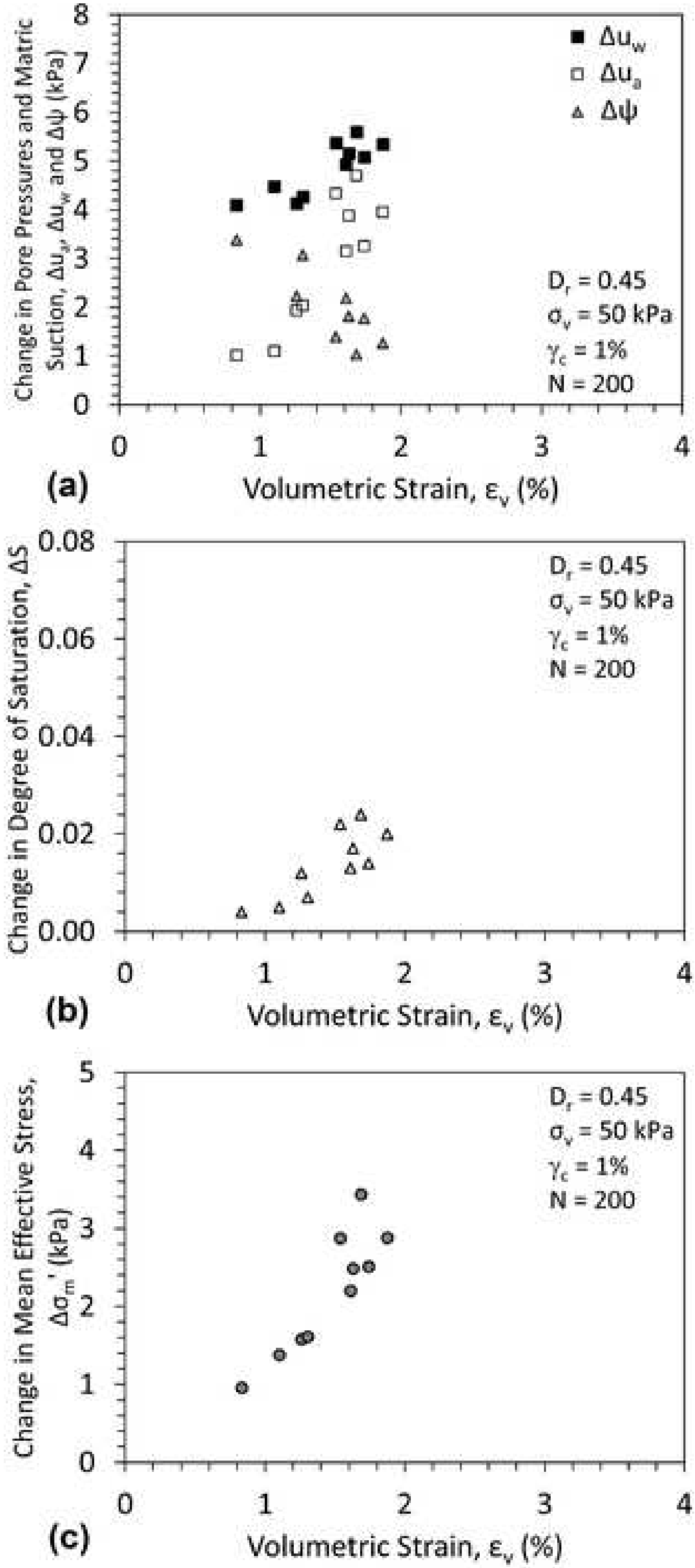

Fig 11

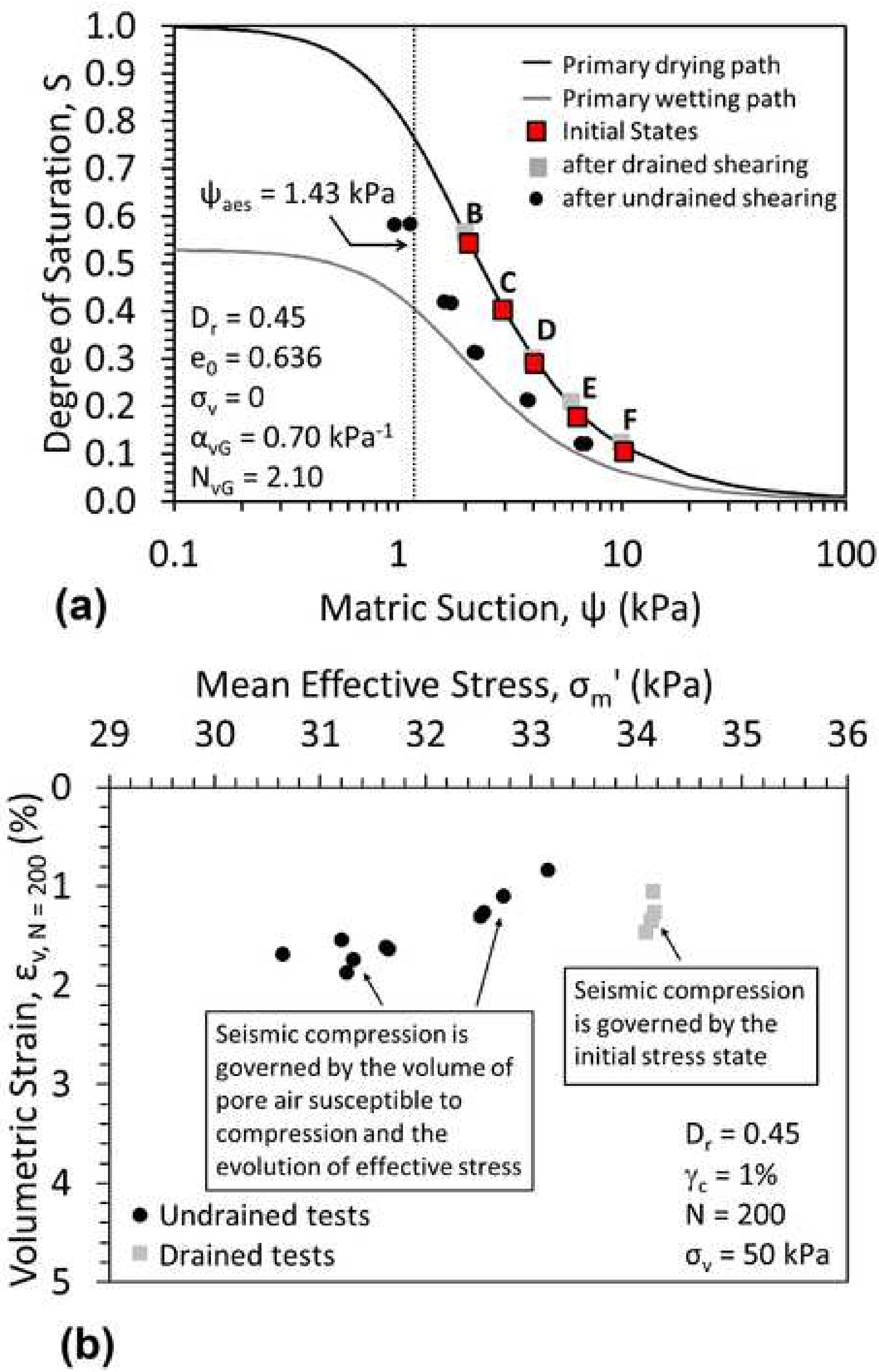
Degree of Saturation, S
1.0
0.9
0.8
0.7
0.6
0.5
0.4
0.3
0.2
0.1
0.0
Primary drying path
Primary wetting path
Initial States
after drained shearing
after undrained shearing
ψaes = 1.43 kPa
B
C
D
E
F
Dr = 0.45
e0 = 0.636
σv = 0
αvG = 0.70 kPa-1
NvG = 2.10
0.1
1
10
100
(a)
Matric Suction, ψ (kPa)
Mean Effective Stress, σm' (kPa)
29
30
31
32
33
34
35
36
Volumetric Strain, εv, N = 200 (%)
0
1
2
3
4
5
Seismic compression is governed by the volume of pore air susceptible to compression and the evolution of effective stress
Seismic compression is governed by the initial stress state
Dr = 0.45
γc = 1%
N = 200
σv = 50 kPa
Undrained tests
Drained tests
(b)

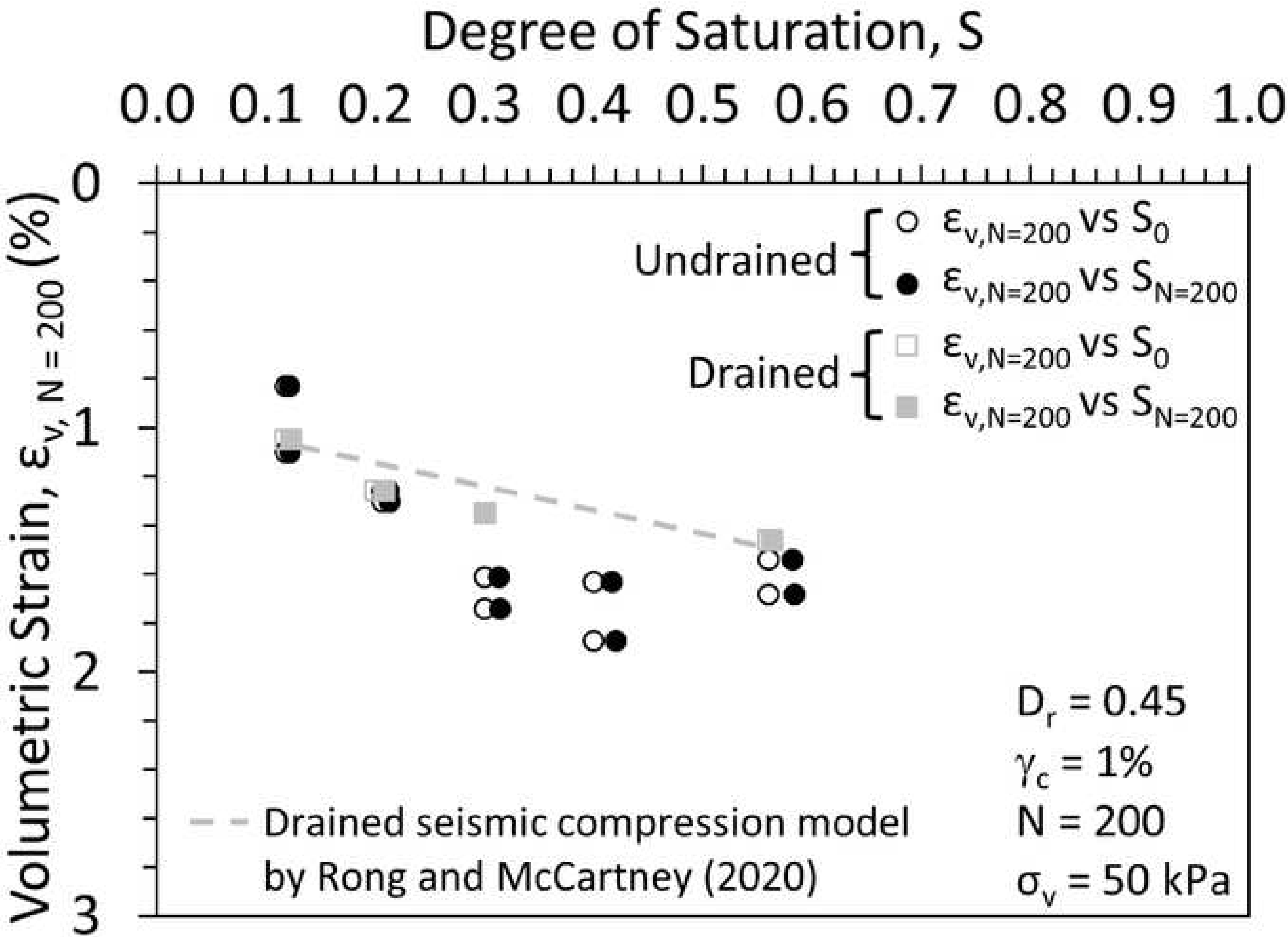

Degree of Saturation, S
0.0 0.1 0.2 0.3 0.4 0.5 0.6 0.7 0.8 0.9 1.0
Volumetric Strain, ε_v, N = 200 (%)
0
1
2
3
Undrained
ε_v,N=200 vs S_0
ε_v,N=200 vs S_N=200
Drained
ε_v,N=200 vs S_0
ε_v,N=200 vs S_N=200
Drained seismic compression model
by Rong and McCartney (2020)
D_r = 0.45
γ_c = 1%
N = 200
σ_v = 50 kPa

LIST OF FIGURE CAPTIONS:

FIG. 1: Schematic view of the specimen housing with suction-saturation control for drained or undrained cyclic shearing of unsaturated sands (dimensions in mm), with the inset showing the differences in boundary conditions for drained and undrained conditions

FIG. 2: Characteristics of the well-graded sand (SW): (a) Particle size distribution curve; (b) SWRC at D_r = 0.45 with initial specimen conditions; (c) SSCC at D_r = 0.45 with initial specimen conditions

FIG. 3: Typical undrained cyclic shearing results for an unsaturated sand specimen with an initial suction of 4 kPa (Specimen D-1): (a) Measured cyclic shear strain; (b) Measured cyclic shear stress; (c) Measured volumetric strain; (d) Measured pore water and air pressures; (e) Matric suction and degree of saturation; (f) Mean effective stress

FIG. 4: Evolutions of hydro-mechanical variables for unsaturated sand specimens with different initial suctions during undrained cyclic shearing (specimen B-1, C-1, D-1, E-1, F-1): (a) Volumetric strain; (b) Degree of saturation; (c) Matric suction; (d) Mean effective stress

FIG. 5: Typical cyclic responses of an unsaturated sand specimen with an initial suction of 4 kPa (Specimen D-1): (a) Volumetric strain vs. shear strain; (b) Volumetric strain vs. vertical effective stress; (c) Cyclic shear stress vs. vertical effective stress; (d) Hysteretic shear stress-strain curves

FIG. 6: Evolution of dynamic properties for sand specimens with different initial degrees of saturation or suctions during undrained cyclic shearing (Specimens A-1, B-1, C-1, D-1, E-1, F-1, G-1): (a) Secant shear modulus vs. cycles; (b) Damping ratio vs. cycles

FIG. 7: Relations between volume change and stress state during undrained cyclic shearing for sand specimens with different initial degrees of saturation (Specimens B-1, C-1, D-1, E-1, F-1,

G-1): (a) Volumetric strain vs. mean effective stress; (b) Replot of the data from these specimens in e-logσ_m' space with oedometer compression test results

FIG. 8: Volumetric strains accumulated after 200 cycles for unsaturated sand specimens: (a) Volumetric strain vs. degree of saturation; (b) Volumetric strain vs. suction

FIG. 9: Changes in the hydraulic parameters and the stress state against the initial saturation: (a) Δu_w, Δu_a and $\Delta\psi$ vs. S_{r0}; (b) ΔS vs. S_{r0}; (c) $\Delta\sigma_m$' vs. S_{r0}

FIG. 10: Changes in the hydraulic parameters and the stress state against the volumetric strains after 200 cycles of undrained cyclic shearing: (a) Δu_w, Δu_a and $\Delta\psi$ vs. ε_v; (b) ΔS vs. ε_v; (c) $\Delta\sigma_m$' vs. ε_v

FIG. 11: Comparison between undrained and drained cyclic shearing tests on unsaturated sand specimens: (a) Movement of the SWRC after N = 200; (b) Volumetric strain vs. mean effective stress after N = 200

FIG. 12: Dependence of the accumulated volumetric strains of the unsaturated specimens with varying degrees of saturation in the funicular regime on the degree of saturation during both drained and undrained cyclic shearing